



# Dynamic Feedback Linearizability of Ingenuity

A.A. 2025 - 2026

Luca Franzin  
Andrea Gravili  
Giuseppe D'Addario  
Federico Tranzocchi  
*Sapienza University of Rome*

# Contents

<b>1</b>	<b>Introduction</b>	<b>3</b>
1.1	The Ingenuity helicopter . . . . .	3
1.1.1	Control . . . . .	4
1.2	Objective . . . . .	5
1.3	Structure . . . . .	5
<b>2</b>	<b>Ingenuity dynamic model</b>	<b>6</b>
2.1	Coordinate frames . . . . .	6
2.2	State and input . . . . .	6
2.3	Equations of motion . . . . .	7
2.3.1	Kinematics . . . . .	7
2.3.2	Translational dynamics . . . . .	8
2.3.3	Rotational dynamics . . . . .	8
2.4	Complete state-space model . . . . .	9
<b>3</b>	<b>Control design</b>	<b>10</b>
3.1	Dynamic feedback linearization . . . . .	10
3.1.1	Ingenuity DFL . . . . .	11
3.2	Control architecture summary . . . . .	14
<b>4</b>	<b>Simulation setup</b>	<b>16</b>
4.1	Simulation environment . . . . .	16
4.2	Model parameters . . . . .	16
4.3	Controller implementation . . . . .	16
4.3.1	Gain tuning . . . . .	16
4.3.2	Actuator saturation . . . . .	17
4.4	Reference trajectories . . . . .	18
4.5	Disturbances . . . . .	18
4.6	Performance metrics . . . . .	19
<b>5</b>	<b>Results</b>	<b>20</b>
5.1	Nominal performance . . . . .	20
5.1.1	Figure-8 trajectory (constant yaw) . . . . .	20
5.1.2	Helix trajectory (spinning yaw) . . . . .	21
5.2	Robustness analysis . . . . .	22
5.2.1	Vertical wind on figure-8 . . . . .	22
5.2.2	3D wind on helix . . . . .	23
5.3	Complex maneuvering . . . . .	25
5.3.1	Ideal patrolling (no wind) . . . . .	25

5.3.2	Patrolling with environmental noise . . . . .	26
<b>6</b>	<b>Conclusion</b>	<b>27</b>
6.1	Summary . . . . .	27
6.2	Future work . . . . .	27

# Chapter 1

## Introduction

The exploration of Mars has been significantly advanced with the success of the NASA Perseverance rover mission, whose primary objective is to search for signs of past microbial life and collect samples of Martian rock and soil. A key component of this mission is the *Ingenuity* helicopter (Figure 1.1), which demonstrates the potential of aerial vehicles for planetary exploration. Ingenuity's flights provide valuable data on the Martian atmosphere and, in general, environmental conditions that can be leveraged for future missions.



Figure 1.1: Ingenuity at Wright Brothers Field on 6 April 2021, its third day of deployment on Mars. Image source: Wikipedia.

### 1.1 The Ingenuity helicopter

Unlike the more common quadrotors, Ingenuity is a *co-axial* helicopter with two counter-rotating rotors stacked on a single mast. This design choice allows for a more compact structure that does not need a tail rotor to counteract torque. Instead of controlling motion through varying the speed of the two rotors, Ingenuity uses a mechanism called *swashplate* [1] (see Figure 1.2) to change the pitch of the rotor blades cyclically and collectively.

- *Cyclic pitch* changes the angle of the blades as they rotate, which tilts the thrust vector allowing to generate the forces and moments needed for horizontal motion (roll and pitch).
- *Collective pitch* adjusts the angle of all blades of a rotor simultaneously, controlling the total magnitude of the thrust for vertical motion.

This actuation method yields flight dynamics that are fundamentally different from those of multi-rotor drones.

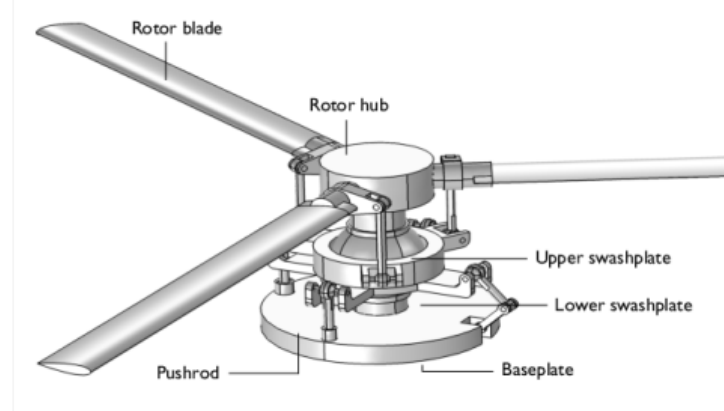


Figure 1.2: A helicopter swashplate mechanism. It translates non-rotating control inputs from the servos into the rotating frame of the rotor blades, controlling both collective and cyclic pitch. Image source: COMSOL Application Gallery.

### 1.1.1 Control

Controlling Ingenuity is a challenging task due to two main reasons. First, the Martian atmosphere is much thinner than Earth's, with a density of about 1% that of sea level on Earth. This results in reduced aerodynamic forces and moments, making it difficult to generate sufficient lift and, in general, it alters the helicopter's flight dynamics. This requires the two rotors to spin at very high speeds (over 2500 RPM) to generate enough lift for takeoff and maneuvering, leading to complex aerodynamic effects [2].

Second, the helicopter's dynamics are nonlinear and coupled. In fact, the forces generated by the rotors depend on the vehicle's orientation, and the translational and rotational motions are linked. While linear controllers have been successfully used for Ingenuity's flight control [1], their performance can be limited, especially during aggressive maneuvers or in the presence of disturbances such as wind gusts. In general, standard linear control techniques tend to struggle in handling these nonlinearities.

#### Dynamic feedback linearization

We adopt an approach from nonlinear control theory known as *dynamic feedback linearization* (DFL) [3] that aims to cancel out the coupled nonlinearities in the system dynamics through feedback, resulting in a decoupled linearized system that can be controlled using linear control methods. The main idea is to find a suitable change of coordinates and a nonlinear control law that cancels out the unwanted nonlinear terms in the dynamics.

The "dynamic" aspect of DFL refers to an extension of the method that is necessary when the control inputs do not immediately affect the outputs, requiring the controller to have its own internal dynamics. As we will show, this is precisely the case for controlling the position of a co-axial helicopter like Ingenuity using the swashplate mechanism.

## 1.2 Objective

The main goal of this project is to formally analyze the dynamic feedback linearizability of the Ingenuity helicopter, design a state feedback controller for *trajectory tracking*, and validate its performance and robustness through turbances and simulations. Specifically, we aim to:

1. Develop a dynamic model of Ingenuity based on Newton-Euler equations, capturing the key dynamics and couplings introduced by the co-axial rotor configuration;
2. analyze such dynamics to determine the conditions under which the system can be linearized using dynamic feedback;
3. design the nonlinear control law that achieves linearization and decoupling;
4. implement a tracking controller for the linearized system;
5. evaluate the performance of our controller in simulation under various scenarios and for different maneuvers.

## 1.3 Structure

The report is organized as follows. In Chapter 2 we present the detailed dynamic model of the Ingenuity helicopter deriving the equations of motion. In Chapter 3 we provide a mathematical formulation of the dynamic feedback linearization technique and derive the specific control law for our system. In Chapter 4 we describe the simulation environment, the implementation details of the controller, and the test scenarios. In Chapter 5 we present the results of our experiments and evaluate the controller's performance. Finally, in Chapter 6 we summarize our findings and discuss potential future work.

# Chapter 2

## Ingenuity dynamic model

In this chapter, we develop the mathematical model of the Ingenuity helicopter using Newton-Euler equations. We start by defining the reference frames and the notation used throughout the report, the state and input vectors of the system, and derive the translational and rotational equations of motion governing the vehicle's flight. The dynamic model derived here is based on the formulation presented in [4] and will serve as the basis for the control system design analyzed in Chapter 3.

### 2.1 Coordinate frames

To describe the motion of Ingenuity, we define two main right-handed coordinate frames:

- The *inertial frame*  $\{I\}$ , which is a fixed non-accelerating frame used as a global reference. Its origin is located at the takeoff point on the Martian surface, and its axes are denoted by  $(x_i, y_i, z_i)$ . We adopt a  $z$ -up convention, with the  $z_i$  axis pointing vertically upwards in the opposite direction of gravity.
- The *body frame*  $\{B\}$ , which is a frame attached to the vehicle with its origin at the center of mass. Its axes  $(x_b, y_b, z_b)$  are aligned with the principal axes of Ingenuity, with  $x_b$  pointing forward,  $y_b$  pointing to the right, and  $z_b$  pointing up along the rotor mast.

The orientation of the body frame with respect to the inertial frame is described by a rotation matrix  $\mathbf{R} \in SO(3)$  which transforms vectors from the body frame to the inertial frame. Such a matrix is parameterized using the ZYX Euler angles convention, defined by the yaw ( $\psi$ ), pitch ( $\theta$ ), and roll ( $\phi$ ) angles:

$$\mathbf{R} = \begin{bmatrix} c_\psi c_\theta & c_\psi s_\theta s_\phi - s_\psi c_\phi & c_\psi s_\theta c_\phi + s_\psi s_\phi \\ s_\psi c_\theta & s_\psi s_\theta s_\phi + c_\psi c_\phi & s_\psi s_\theta c_\phi - c_\psi s_\phi \\ -s_\theta & c_\theta s_\phi & c_\theta c_\phi \end{bmatrix} \quad (2.1)$$

where  $c_\alpha = \cos(\alpha)$  and  $s_\alpha = \sin(\alpha)$ , for any angle  $\alpha$ .

### 2.2 State and input

The *state* of the system captures its complete dynamic condition at any given time. The *input* vector represents the control commands used to control the system.

**State vector** The state of the Ingenuity helicopter is described by a 12-dimensional vector  $\xi \in \mathbb{R}^{12}$ , which includes its position, linear velocity, orientation, and angular velocity:

$$\xi = \begin{pmatrix} \mathbf{P} \\ \mathbf{V}^b \\ \Theta \\ \omega \end{pmatrix} \in \mathbb{R}^{12} \quad (2.2)$$

where:

- $\mathbf{P} = (x, y, z)^T \in \mathbb{R}^3$  is the position of the vehicle's center of mass in the inertial frame  $\{I\}$ ;
- $\mathbf{V}^b = (V_x^b, V_y^b, V_z^b)^T = (u, v, w)^T \in \mathbb{R}^3$  is the linear velocity of the center of mass expressed in the body frame  $\{B\}$ ;
- $\Theta = (\phi, \theta, \psi)^T \in \mathbb{R}^3$  are the Euler angles representing the orientation of the body frame  $\{B\}$  with respect to the inertial frame  $\{I\}$ ;
- $\omega = (p, q, r)^T \in \mathbb{R}^3$  is the angular velocity of the vehicle expressed in the body frame  $\{B\}$ .

**Input vector** Ingenuity is controlled via the net thrust produced by its two rotors and the net torques applied to the body. We define a 4-dimensional input vector  $\mathbf{u} \in \mathbb{R}^4$  that abstracts the complex swashplate mechanism and rotor dynamics into the following components:

$$\mathbf{u} = \begin{pmatrix} F_T \\ \tau_\phi \\ \tau_\theta \\ \tau_\psi \end{pmatrix} \in \mathbb{R}^4 \quad (2.3)$$

where:

- $F_T$  is the magnitude of the total thrust force acting along the body  $z_b$  axis;
- $\tau_\phi$ ,  $\tau_\theta$ , and  $\tau_\psi$  are the net control torques applied around the body axes  $x_b, y_b, z_b$ , respectively.

## 2.3 Equations of motion

The dynamics are separated into *kinematic* and *dynamic* equations: kinematics describe how the position and orientation evolve based on the velocities, while dynamics describe how the velocities change based on the applied forces and torques.

### 2.3.1 Kinematics

The kinematic equations describe the geometry of motion without considering the forces that cause it.

The rate of change of the inertial position is the linear velocity in the inertial frame, which is obtained by transforming the body-frame velocity using the rotation matrix in Eq. (2.1):

$$\dot{\mathbf{P}} = \mathbf{R}\mathbf{V}^b \quad (2.4)$$

The rate of change of the Euler angles is related to the body-frame angular velocity through the following transformation:

$$\begin{pmatrix} \dot{\phi} \\ \dot{\theta} \\ \dot{\psi} \end{pmatrix} = \dot{\Theta} = \mathbf{W}(\Theta)\boldsymbol{\omega} = \begin{pmatrix} 1 & s_\phi t_\theta & c_\phi t_\theta \\ 0 & c_\phi & -s_\phi \\ 0 & s_\phi/c_\theta & c_\phi/c_\theta \end{pmatrix} \begin{pmatrix} p \\ q \\ r \end{pmatrix} \quad (2.5)$$

where  $t_\alpha = \tan(\alpha)$ , for any angle  $\alpha$ .

### 2.3.2 Translational dynamics

The translational dynamics are derived from *Newton's second law*, which we express in the body frame  $\{B\}$ :

$$m\dot{\mathbf{V}}^b = \mathbf{F}_{\text{tot}}^b - m\boldsymbol{\omega} \times \mathbf{V}^b \quad (2.6)$$

where  $m$  is the mass of the vehicle, and the term  $m(\boldsymbol{\omega} \times \mathbf{V}^b)$  is the Coriolis force that arises from differentiating the velocity in a rotating frame. The total force  $\mathbf{F}_{\text{tot}}^b$  in the body frame is the sum of the thrust force, gravity, and aerodynamic drag:

$$\mathbf{F}_{\text{tot}}^b = \mathbf{F}_{\text{thrust}}^b + \mathbf{F}_{\text{gravity}}^b + \mathbf{F}_{\text{drag}}^b \quad (2.7)$$

In detail:

- The *thrust force* is the force generated by the two rotors acting along the positive  $z_b$  axis of the body frame  $\{B\}$ :

$$\mathbf{F}_{\text{thrust}}^b = \begin{pmatrix} 0 \\ 0 \\ F_T \end{pmatrix} \quad (2.8)$$

- The *gravitational force* is the weight of the vehicle acting downwards in the inertial frame  $\{I\}$  rotated into the body frame  $\{B\}$  using the transpose of the rotation matrix in Eq. (2.1):

$$\mathbf{F}_{\text{gravity}}^b = \mathbf{R}^T \mathbf{F}_{\text{gravity}}^i = \mathbf{R}^T \begin{pmatrix} 0 \\ 0 \\ -mg \end{pmatrix} \quad (2.9)$$

- The *aerodynamic drag force* is modeled as a simple linear damping proportional to the body-frame velocity:

$$\mathbf{F}_{\text{drag}}^b = -\mathbf{A}_{\text{trans}} \mathbf{V}^b \quad (2.10)$$

where  $\mathbf{A}_{\text{trans}}$  is a diagonal matrix containing the translational drag coefficients along each body axis (see Chapter 4).

### 2.3.3 Rotational dynamics

The rotational dynamics are derived from *Euler's equation* for rigid body rotation, expressed in the body frame  $\{B\}$ :

$$\mathbf{I}\dot{\boldsymbol{\omega}} = \boldsymbol{\tau}_{\text{tot}}^b - \boldsymbol{\omega} \times \mathbf{I}\boldsymbol{\omega} \quad (2.11)$$

where  $\mathbf{I}$  is the inertia matrix, and the term  $\boldsymbol{\omega} \times \mathbf{I}\boldsymbol{\omega}$  represents the gyroscopic torques due to the rotating frame. The total torque  $\boldsymbol{\tau}_{\text{tot}}^b$  in the body frame is the sum of the control torques and aerodynamic damping torques:

$$\boldsymbol{\tau}_{\text{tot}}^b = \boldsymbol{\tau}_{\text{control}}^b + \boldsymbol{\tau}_{\text{drag}}^b \quad (2.12)$$

In detail:

- The *control torques* are the torques generated by the swashplate mechanism around each body axis, and are given by the control inputs in Eq. (2.3):

$$\boldsymbol{\tau}_{\text{control}}^b = \begin{pmatrix} \tau_\phi \\ \tau_\theta \\ \tau_\psi \end{pmatrix} \quad (2.13)$$

- The *aerodynamic damping torques* are modeled as linear damping opposing the angular velocity:

$$\boldsymbol{\tau}_{\text{drag}}^b = -\mathbf{A}_{\text{rot}}\boldsymbol{\omega} \quad (2.14)$$

where  $\mathbf{A}_{\text{rot}}$  is a diagonal matrix containing the rotational drag coefficients around each body axis (see Chapter 4).

## 2.4 Complete state-space model

Combining the kinematic and dynamic equations, we obtain the complete *nonlinear* state-space model of the Ingenuity helicopter in the form  $\dot{\boldsymbol{\xi}} = \mathbf{f}(\boldsymbol{\xi}, \mathbf{u})$ :

$$\dot{\boldsymbol{\xi}} = \begin{pmatrix} \dot{\mathbf{P}} \\ \dot{\mathbf{V}}^b \\ \dot{\boldsymbol{\Theta}} \\ \dot{\boldsymbol{\omega}} \end{pmatrix} = \begin{pmatrix} \mathbf{R}\mathbf{V}^b \\ \frac{1}{m} (\mathbf{F}_{\text{thrust}}^b + \mathbf{F}_{\text{gravity}}^b + \mathbf{F}_{\text{drag}}^b) - \boldsymbol{\omega} \times \mathbf{V}^b \\ \mathbf{W}(\boldsymbol{\Theta})\boldsymbol{\omega} \\ \mathbf{I}^{-1} (\boldsymbol{\tau}_{\text{control}}^b + \boldsymbol{\tau}_{\text{drag}}^b - \boldsymbol{\omega} \times \mathbf{I}\boldsymbol{\omega}) \end{pmatrix} \quad (2.15)$$

We will be using this set of 12 coupled nonlinear differential equations as the basis for our analysis of dynamic feedback linearization in Chapter 3.

# Chapter 3

## Control design

This chapter details the design of a nonlinear controller for the Ingenuity helicopter model developed in Chapter 2. Due to the underactuated and coupled nature of its dynamics, standard linear control techniques are not suitable for achieving trajectory tracking. We therefore employ the technique of *dynamic feedback linearization* (DFL) to cancel the system's inherent nonlinearities and achieve a linear input-output mapping.

The objective is to design a control law for the input vector  $\mathbf{u}$  defined in Eq. (2.3) that forces the position  $\mathbf{P}(t)$  and yaw angle  $\psi(t)$  of Ingenuity to track a desired smooth trajectory  $(\mathbf{P}_d(t), \psi_d(t))$ . To achieve this, we will first analyze the system's input-output relationship to determine the *relative degree* of each output with respect to the inputs. Then, we will design a *dynamic compensator* with an internal state  $\zeta$  to augment the system and achieve full relative degree, so as to get a feedback linearizing control law. Finally, we will design an *outer-loop* linear tracking controller to stabilize the tracking error for the linearized system.

### 3.1 Dynamic feedback linearization

For a general nonlinear system of the form  $\dot{\xi} = \mathbf{f}(\xi) + \mathbf{G}(\xi)\mathbf{u}$  with output  $\mathbf{y} = \mathbf{h}(\xi)$ , the goal of feedback linearization is to find a *coordinate transformation* and a control law that renders the input-output map linear. This is achieved by differentiating each output  $y_i$  until at least one input  $u_j$  appears. The number of differentiation required is called the *relative degree*  $r_i$  of the output  $y_i$ .

If the total relative degree  $r = \sum r_i$  is less than the dimension of the state  $n$ , the system has residual internal dynamics (*zero dynamics*) that may be unstable. On the other hand, if  $r = n$  the system can be fully linearized.

When the control inputs do not appear in a way that allows for direct cancellation of nonlinearities, that is when the *decoupling matrix* is singular, we introduce a *dynamic compensator* with its own internal state  $\zeta$  and dynamics  $\dot{\zeta}$ . This involves augmenting the system with integrators on the input channels, which leads to an increased dimension of the state space to match the total relative degree.

### 3.1.1 Ingenuity DFL

We apply the DFL framework to the dynamics of Ingenuity. The outputs we want to control are the position  $\mathbf{P} = (x, y, z)^T$  and yaw angle  $\psi$ , so we define the output vector as:

$$\mathbf{y} = \begin{pmatrix} x \\ y \\ z \\ \psi \end{pmatrix} \quad (3.1)$$

We can now differentiate each component of the output vector  $\mathbf{y}$  until a component of the input vector  $\mathbf{u}$  appears, and determine the corresponding relative degree.

#### Yaw channel

The yaw dynamics are governed by the rotational kinematics and the rotational dynamics. Differentiating the yaw angle  $\psi$  once gives:

$$\dot{\psi}_4 = \dot{\psi} = \frac{\sin \phi}{\cos \theta} q + \frac{\cos \phi}{\cos \theta} r$$

This expression depends only on the states  $\phi, \theta, q, r$  and no inputs appear, so we differentiate again:

$$\ddot{\psi} = \underbrace{(s_\phi \sec \theta) \dot{q} + (c_\phi \sec \theta) \dot{r}}_{\text{input-dependent}} + \underbrace{(\dot{\phi} c_\phi \sec \theta + s_\phi \dot{\theta} \sec \theta \tan \theta) q + (-\dot{\phi} s_\phi \sec \theta + c_\phi \dot{\theta} \sec \theta \tan \theta) r}_{\text{state-dependent} = \mathbf{f}_\psi(\xi)}$$

where  $\mathbf{f}(\xi)$  is the *drift* term, and the input-dependent part can be expressed as:

$$(0 \quad s_\phi \sec \theta \quad c_\phi \sec \theta) \dot{\omega}$$

where  $\dot{\omega}$  is given by the rotational dynamics in Eq. (2.11). Substituting this expression, we obtain:

$$\ddot{\psi} = \mathbf{f}_\psi(\xi) + (0 \quad s_\phi \sec \theta \quad c_\phi \sec \theta) \mathbf{I}^{-1} (\boldsymbol{\tau}_{\text{control}}^b + \boldsymbol{\tau}_{\text{drag}}^b - \boldsymbol{\omega} \times \mathbf{I} \boldsymbol{\omega}) \quad (3.2)$$

We see that the control torques  $\boldsymbol{\tau}_{\text{control}}^b$  appear linearly (in particular, the two inputs  $u_3 = \tau_\theta$  and  $u_4 = \tau_\psi$ ), so the relative degree of the yaw channel is  $r_\psi = 2$ .

#### Position channel

The position dynamics reveal that the system is *underactuated*. From the translational kinematics in Eq. 2.4, we have:

$$\dot{\mathbf{P}} = \mathbf{R}(\Theta) \mathbf{V}^b$$

which is independent of the inputs. We therefore differentiate twice:

$$\begin{aligned} \ddot{\mathbf{P}} &= \dot{\mathbf{R}} \mathbf{V}^b + \mathbf{R} \dot{\mathbf{V}}^b \\ &= \underline{\mathbf{R} \mathbf{S}(\boldsymbol{\omega}) \mathbf{V}^b} + \mathbf{R} \left[ \frac{1}{m} (\mathbf{F}_{\text{thrust}}^b + \mathbf{F}_{\text{gravity}}^b + \mathbf{F}_{\text{drag}}^b) - \boldsymbol{\omega} \times \mathbf{V}^b \right] \\ &= \frac{1}{m} \mathbf{R} \begin{pmatrix} 0 \\ 0 \\ \mathbf{F}_T \end{pmatrix} + \begin{pmatrix} 0 \\ 0 \\ -g \end{pmatrix} - \frac{1}{m} \mathbf{R} \mathbf{A}_{\text{trans}} \mathbf{V}^b \end{aligned}$$

The input  $F_T$  appears, but the control inputs  $\tau_\phi, \tau_\theta$  do not. We must continue differentiating:

$$P^{(3)} = \frac{d}{dt} \left[ \frac{F_T}{m} \mathbf{R} \mathbf{e}_3 - g \mathbf{e}_3 + \frac{1}{m} \mathbf{R} \mathbf{F}_{\text{drag}}^b \right]$$

The time derivative of the second term is zero. The third term depends on  $\mathbf{V}^b$  and  $\boldsymbol{\omega}$ , but not on its derivative  $\dot{\boldsymbol{\omega}}$ , and thus will not introduce any new input. As for the first term, we have:

$$\frac{d}{dt} \left[ \frac{F_T}{m} \mathbf{R} \mathbf{e}_3 \right] = \frac{\cancel{\dot{F}_T}}{m} \mathbf{R} \mathbf{e}_3 + \frac{F_T}{m} \dot{\mathbf{R}} \mathbf{e}_3$$

The term  $\dot{F}_T$  appears, which is not a control input. We therefore differentiate one last time:

$$P^{(4)} = \frac{d}{dt} \left[ \frac{\dot{F}_T}{m} \mathbf{R} \mathbf{e}_3 + \frac{F_T}{m} \mathbf{R} \mathbf{S}(\boldsymbol{\omega}) \mathbf{e}_3 + \dots \right]$$

The first term gives:

$$\frac{d}{dt} \left[ \frac{\dot{F}_T}{m} \mathbf{R} \mathbf{e}_3 \right] = \frac{\ddot{F}_T}{m} \mathbf{R} \mathbf{e}_3 + \frac{\dot{F}_T}{m} \dot{\mathbf{R}} \mathbf{e}_3$$

Again, we have a non-input term  $\ddot{F}_T$ . The second term gives:

$$\frac{d}{dt} \left[ \frac{F_T}{m} \mathbf{R} \mathbf{S}(\boldsymbol{\omega}) \mathbf{e}_3 \right] = \dots + \frac{F_T}{m} \mathbf{R} \mathbf{S}(\dot{\boldsymbol{\omega}}) \mathbf{e}_3$$

where  $\dot{\boldsymbol{\omega}}$  appears, which is a direct linear function of the input torques  $\boldsymbol{\tau}_{\text{control}}^b$ . Therefore, the relative degree of each position channel is  $r_x = r_y = r_z = 4$ .

## Dynamic compensator

The appearance of  $\ddot{F}_T$  in  $P^{(4)}$  indicates that the thrust input  $F_T$  does not directly influence the outputs in a way that allows for cancellation of nonlinearities. We need to introduce a dynamic compensator for the thrust channel, augmenting the state of the system with two additional controller states:

$$\boldsymbol{\zeta} = \begin{pmatrix} \zeta_1 \\ \zeta_2 \end{pmatrix} = \begin{pmatrix} F_T \\ \dot{F}_T \end{pmatrix} \quad (3.3)$$

The dynamics of the compensator are given by a simple integrator chain driven by a new *virtual input*  $v_T$ :

$$\dot{\boldsymbol{\zeta}} = \begin{pmatrix} \dot{\zeta}_1 \\ \dot{\zeta}_2 \end{pmatrix} = \begin{pmatrix} \zeta_2 \\ v_T \end{pmatrix} = \begin{pmatrix} \dot{F}_T \\ \ddot{F}_T \end{pmatrix} \quad (3.4)$$

The thrust  $F_T$  applied to Ingenuity is now treated as a state variable  $\zeta_1$  that evolves according to the compensator dynamics. The extended state of the system is  $(\boldsymbol{\xi}, \boldsymbol{\zeta}) \in \mathbb{R}^{14}$ .

## Linearizing control law

The total relative degree of the augmented system is now:

$$r = r_x + r_y + r_z + r_\psi = 4 + 4 + 4 + 2 = 14$$

which equals the dimension of the extended state space ( $n_{\text{ext}} = 12 + 2 = 14$ ). Therefore, the system is fully state linearizable with no zero dynamics.

We define the extended input vector as:

$$\tilde{\mathbf{u}} = \begin{pmatrix} \ddot{F}_T \\ \tau_\phi \\ \tau_\theta \\ \tau_\psi \end{pmatrix} \quad (3.5)$$

The dynamics of the output can now be expressed in the standard affine form:

$$\begin{pmatrix} P^{(4)} \\ \ddot{\psi} \end{pmatrix} = \mathbf{l}(\xi, \zeta) + \mathbf{J}(\xi, \zeta)\tilde{\mathbf{u}} \quad (3.6)$$

where  $\mathbf{l}(\xi, \zeta)$  is the drift vector containing all state-dependent terms, and  $\mathbf{J}(\xi, \zeta)$  is the  $4 \times 4$  decoupling matrix.

**Decoupling matrix  $\mathbf{J}$**  The decoupling matrix  $\mathbf{J}$  contains the coefficients of the extended inputs  $\tilde{\mathbf{u}}$  in the output derivative equations. By carrying out the differentiations in the previous section, we can identify its components:

$$\mathbf{J}(\xi, \zeta) = \left[ \begin{array}{c|c} \frac{1}{m} \mathbf{R} \mathbf{e}_3 & -\frac{F_T}{m} \mathbf{R} \mathbf{S}(\mathbf{e}_3) \mathbf{I}^{-1} \\ \mathbf{0}_{1 \times 1} & (0 \ s_\phi \sec \theta \ c_\phi \sec \theta) \mathbf{I}^{-1} \end{array} \right] \quad (3.7)$$

The block  $\mathbf{J}_{11}$  is a  $3 \times 1$  vector representing the effect of  $\ddot{F}_T$  on  $P^{(4)}$ . The block  $\mathbf{J}_{12}$  is a  $3 \times 3$  matrix representing the effect of the control torques on  $P^{(4)}$ . The block  $\mathbf{J}_{21}$  is zero, since the yaw acceleration is independent of the thrust dynamics  $\ddot{F}_T$ . The block  $\mathbf{J}_{22}$  is a  $1 \times 3$  vector representing the effect of the control torques on  $\ddot{\psi}$ .

This decoupling matrix is dependent on  $F_T$  and becomes singular if  $F_T = 0$ . In this condition, the torques have no effect on the position, and the system is uncontrollable. In practice, we implement a check to disable the controller if the thrust magnitude approaches zero.

**Drift vector  $\mathbf{l}$**  The drift vector  $\mathbf{l}$  contains all the state-dependent terms from the differentiation that do not multiply the extended inputs. It can be partitioned as:

$$\mathbf{l} = \begin{pmatrix} \mathbf{l}_{\text{pos}} \\ l_\psi \end{pmatrix}$$

The yaw drift  $l_\psi$  is derived from Eq. (3.2):

$$l_\psi(\xi) = (\dot{\phi}c_\phi \sec \theta + s_\phi \dot{\theta} \sec \theta \tan \theta)q + (-\dot{\phi}s_\phi \sec \theta + c_\phi \dot{\theta} \sec \theta \tan \theta)r \quad (3.8)$$

The position drift  $\mathbf{l}_{\text{pos}}$  contains all terms from the fourth derivative of position that are not part of the decoupling matrix. Its full expression is complex, so we highlight only its main components:

$$\mathbf{l}_{\text{pos}} = \frac{2\dot{F}_T}{m} \mathbf{R} \mathbf{S}(\boldsymbol{\omega}) \mathbf{e}_3 + \frac{F_T}{m} \mathbf{R} \mathbf{S}^2(\boldsymbol{\omega}) \mathbf{e}_3 + \frac{F_T}{m} \mathbf{R} \mathbf{S}(\dot{\boldsymbol{\omega}}_{\text{drift}}) \mathbf{e}_3 + \dots \quad (3.9)$$

where  $\dot{\boldsymbol{\omega}}_{\text{drift}} = \mathbf{I}^{-1}(\boldsymbol{\tau}_{\text{drag}}^b - \boldsymbol{\omega} \times \mathbf{I}\boldsymbol{\omega})$  is the part of the angular acceleration not caused by control inputs. The ellipsis represents higher-order drag terms which are often simplified in implementation.

**Control law** The linearizing control law is chosen to cancel these complex terms:

$$\tilde{\mathbf{u}} = \mathbf{J}^{-1}(\xi, \zeta) [\mathbf{v} - \mathbf{l}(\xi, \zeta)] \quad (3.10)$$

where  $\mathbf{v} = (v_1, v_2, v_3, v_4)^T$  is the new simplified input vector. Applying this control law transforms the input-output dynamics into a set of decoupled linear integrator chains:

$$\begin{cases} x^{(4)} = v_1 \\ y^{(4)} = v_2 \\ z^{(4)} = v_3 \\ \ddot{\psi} = v_4 \end{cases} \quad (3.11)$$

### Outer-loop tracking controller

The final step is to design the input  $\mathbf{v}$  to ensure the tracking errors converge to zero. Let the position error be  $\mathbf{e}_P = \mathbf{P}_d - \mathbf{P}$  and the yaw error be  $e_\psi = \psi_d - \psi$ . For the fourth-order position dynamics, we design a controller with feedforward and state feedback on the error dynamics:

$$v_{1,2,3} = \mathbf{P}_d^{(4)} + \mathbf{K}_3 e_P^{(3)} + \mathbf{K}_2 \ddot{\mathbf{e}}_P + \mathbf{K}_1 \dot{\mathbf{e}}_P + \mathbf{K}_0 \mathbf{e}_P \quad (3.12)$$

where  $v_{1,2,3} = (v_1, v_2, v_3)^T$  and  $\mathbf{K}_i = \text{diag}(k_{i,x}, k_{i,y}, k_{i,z})$  are diagonal gain matrices.

For the second-order yaw dynamics, we use a PD controller with feedforward:

$$v_4 = \ddot{\psi}_d + k_{d,\psi} \dot{\psi}_d + k_{p,\psi} e_\psi \quad (3.13)$$

The gains in Eqs. (3.12) and (3.13) are chosen to place the poles of the respective error characteristic equations in the left-half of the complex plane, ensuring exponential convergence of the tracking errors to zero.

## 3.2 Control architecture summary

The complete control architecture is shown in Figure 3.1. The outer loop computes the virtual input  $\mathbf{v}$  based on the tracking error. The inner loop computes the state-dependent terms  $\mathbf{l}$  and  $\mathbf{J}$  and uses the DFL law (3.10) to calculate the extended inputs  $\tilde{\mathbf{u}}$ . The torque commands are sent to Ingenuity, while the thrust rate command  $v_T$  is integrated through the dynamic compensator to produce the thrust input  $F_T$ .

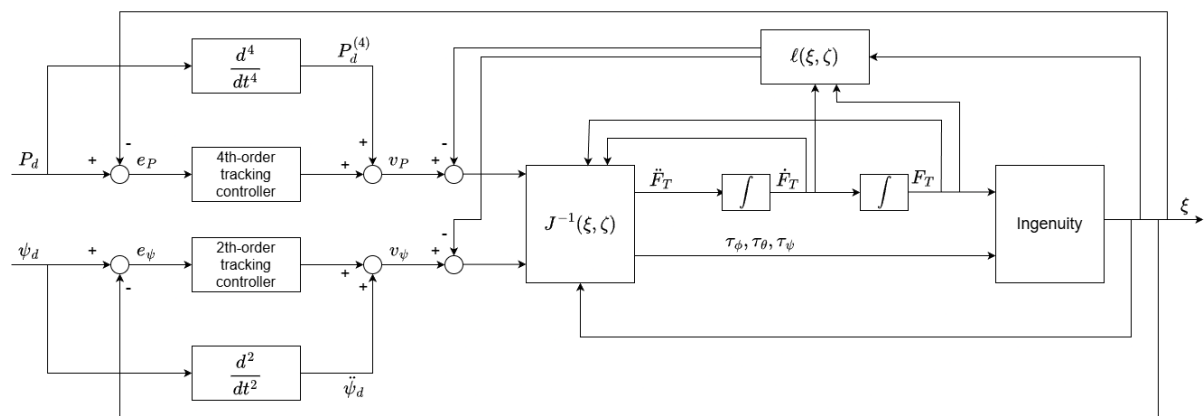


Figure 3.1: Block scheme of the complete DFL control system.

# Chapter 4

## Simulation setup

In this chapter, we describe the simulation environment used to validate the control law computed in Chapter 3. We define the physical parameters of the Ingenuity helicopter, the controller tuning, the reference trajectories used for testing, the external disturbances applied to check robustness, and the performance metrics used to evaluate the results.

### 4.1 Simulation environment

The simulation is implemented in MATLAB. Since the system dynamics derived in Chapter 2 are nonlinear and continuous in time, we use a standard numerical solver for ordinary differential equations (`ode15s`) to integrate the system dynamics. The complete source code for the project, including the dynamic model and the controller implementation, is available on GitHub<sup>1</sup>.

All the simulations are run with a variable time step to ensure numerical stability, but the results are analyzed and plotted over a fixed time span of  $T = 30$  seconds. The initial condition for all simulations corresponds to Ingenuity being on the ground (zero altitude) and the rotors spinning to generate a thrust equal to the vehicle's weight (hovering condition), to simulate a realistic takeoff scenario.

### 4.2 Model parameters

The physical parameters used in the simulation represent the Ingenuity helicopter operating in the Martian environment. The mass and gravity acceleration are taken from the mission data [1]. The inertia tensor is approximated as a diagonal matrix, and the aerodynamic and drag coefficients are estimated to provide a realistic damping effect. Table 4.1 summarizes these parameters.

### 4.3 Controller implementation

#### 4.3.1 Gain tuning

The dynamic feedback linearization controller transforms the nonlinear system into decoupled chains of linear integrators. We stabilize these chains by assigning the poles of the error dy-

---

<sup>1</sup>[https://github.com/yvhem/ingenuity\\_dynamic\\_feedback\\_linearization/tree/main](https://github.com/yvhem/ingenuity_dynamic_feedback_linearization/tree/main)

Table 4.1: Physical parameters of the Ingenuity model.

Parameter	Symbol	Value
Mass	$m$	1.8 kg
Mars Gravity	$g$	3.69 m/s <sup>2</sup>
Inertia ( $x$ -axis)	$I_{xx}$	0.02 kg·m <sup>2</sup>
Inertia ( $y$ -axis)	$I_{yy}$	0.02 kg·m <sup>2</sup>
Inertia ( $z$ -axis)	$I_{zz}$	0.03 kg·m <sup>2</sup>
Translational drag	$A_{\text{trans}}$	diag(0.05, 0.05, 0.1) N·s/m
Rotational drag	$A_{\text{rot}}$	diag(0.01, 0.01, 0.05) N·m·s

namics.

For the position subsystem, which has a relative degree of  $r = 4$ , the error dynamics are described by the linear differential equation:

$$e^{(4)} + k_3 e^{(3)} + k_2 \ddot{e} + k_1 \dot{e} + k_0 e = 0$$

To ensure a fast response with no overshoot, we placed all four poles at  $\lambda = -2$  on the real axis. By expanding the characteristic polynomial  $(s + 2)^4$ , we obtained the following gains:

$$\mathbf{k}_p = [k_0, k_1, k_2, k_3] = [16, 32, 24, 8]$$

These scalars define the diagonal gain matrices used in Eq. (3.12) as  $\mathbf{K}_i = k_i \mathbf{I}_3$ , ensuring identical behavior for the  $x, y, z$  axes.

For the yaw subsystem ( $r = 2$ ), we selected proportional and derivative gains to ensure stable tracking:

$$\mathbf{k}_\psi = [k_{p,\psi}, k_{d,\psi}] = [4, 4]$$

### 4.3.2 Actuator saturation

Real actuators cannot produce infinite forces and torques. To make the simulation realistic, we implemented saturation limits on the control inputs based on the known capabilities of Ingenuity's rotors [1].

**Thrust limits** The thrust produced by the rotors is limited by the rotational speed and the atmospheric density. The thrust-to-weight ratio (TWR) of Ingenuity is between 1.3 and 1.6; we selected a nominal maximum limit of 145%:

$$F_{\max} = 1.45 \cdot mg \approx 9.63 \text{ N}$$

We also enforced a minimum thrust limit of  $F_{\min} = 0.3mg$  to prevent the total thrust from reaching zero, which would cause a singularity in the decoupling matrix  $\mathbf{J}$  (see Chapter 3).

**Torque limits** The control torques  $\tau_\phi, \tau_\theta, \tau_\psi$  are saturated at  $\pm 0.05$  Nm to represent the physical limits of the cyclic and collective pitch mechanism.

## 4.4 Reference trajectories

We define a set of reference trajectories to test the performance of the controller under different conditions. They are chosen so as to evaluate the controller's ability to track both simple and smooth paths, as well as to more aggressive maneuvers.

The controller requires the reference to be smooth up to the fourth derivative (snap) for the position; therefore, all trajectories are generated analytically or via polynomials.

**Box trajectory** This trajectory simulates a patrol mission: the helicopter takes off to an altitude of 5 meters and then follows a square path with a side length of 10 meters. The motion along each segment is generated using quintic polynomials to ensure smooth transitions in position, velocity, acceleration, jerk, and snap. The yaw angle is kept constant at zero throughout the trajectory.

**Helix trajectory** This trajectory requires the helicopter to ascend while performing a circular motion. It is defined analytically as:

$$\begin{cases} x_d(t) = R \cos(\omega_{\text{ref}} t) \\ y_d(t) = R \sin(\omega_{\text{ref}} t) \\ z_d(t) = \min(v_z t, z_{\max}) \end{cases}$$

where the radius is  $R = 2$  m, the angular rate is  $\omega_{\text{ref}} = 0.5$  rad/s, and the vertical velocity is  $v_z = 0.2$  m/s.

**Figure-8 trajectory** This trajectory forces the helicopter to track a figure-8 path at a constant altitude of 5 meters. The planar equations are:

$$\begin{cases} x_d(t) = A \cos(\omega_{\text{ref}} t) \\ y_d(t) = \frac{A}{2} \sin(2\omega_{\text{ref}} t) \\ z_d(t) = z_{\text{ref}} \end{cases} \quad (4.1)$$

where the scale is  $A = 3.0$  m and the frequency is  $\omega_{\text{ref}} = 0.4$  rad/s.

## 4.5 Disturbances

To verify the robustness of the controller, we simulate an external wind gust disturbance. The wind is modeled as a constant force vector  $\mathbf{F}_{\text{wind}}$  acting on the center of mass in the inertial frame.

The disturbance can be configured in terms of:

- *Direction*: the wind can act along any combination of the  $x, y, z$  inertial axes.
- *Intensity*: a randomized magnitude within a specified range (e.g.,  $\pm 2$  N) is applied to the active axes.
- *Timing*: The wind is active only during a specific time window  $[t_{\text{start}}, t_{\text{end}}]$ , typically set to  $t \in [10, 20]$  s to observe the response of the controller.

In the equations of motion, this force is rotated into the body frame and added to the total force:

$$\mathbf{F}_{\text{tot}}^b = \mathbf{F}_{\text{thrust}}^b + \mathbf{F}_{\text{gravity}}^b + \mathbf{F}_{\text{drag}}^b + \mathbf{R}^T \mathbf{F}_{\text{wind}} \quad (4.2)$$

Since the DFL controller relies on model cancellation, this external force acts as an unmodeled disturbance that the outer linear feedback loop must reject.

## 4.6 Performance metrics

To quantitatively evaluate the controller, we compute the following metrics based on the discrete simulation data sampled at time steps  $t_k$ , for  $k = 1, \dots, N$ .

**Robustness to disturbances** To assess the controller's ability to reject unmodeled dynamics, we compute the maximum tracking error specifically during the wind gust interval ( $t \in [t_{\text{start}}, t_{\text{end}}]$  s):

$$e_{\text{gust}} = \max_{t_k \in [t_{\text{start}}, t_{\text{end}}]} \|e_P(t_k)\| \quad (4.3)$$

**Actuator saturation** We evaluate the *feasibility* of the control effort by calculating the percentage of flight time where the thrust input reached its physical saturation limits ( $F_{\min}$  or  $F_{\max}$ ):

$$S\% = \frac{N_{\text{sat}}}{N} \cdot 100 \quad (4.4)$$

A non-zero value indicates that the controller requested more power than the actuators could provide, leading to unavoidable tracking degradation.

# Chapter 5

## Results

In this chapter, we present the simulation results obtained using the control architecture described in Chapter 3 and the setup defined in Chapter 4. The validation strategy is divided into three parts:

1. *Nominal performance*: evaluation of the tracking accuracy in ideal conditions to verify the exact cancellation of nonlinearities.
2. *Robustness analysis*: assessment of the controller's ability to reject external disturbances while tracking trajectories.
3. *Complex maneuvers*: analysis of a "patrol" mission (box trajectory) involving sharp turns and stops, both in the absence and presence of wind disturbances.

### 5.1 Nominal performance

We first evaluate the controller in ideal conditions (no wind, perfect model knowledge). If the model is exact, the nonlinearities should be perfectly cancelled, resulting in linear error dynamics and near-zero tracking error.

#### 5.1.1 Figure-8 trajectory (constant yaw)

In this scenario, the helicopter follows the figure-8 path at a constant altitude and fixed heading ( $\psi = 0$ ), forcing Ingenuity to fly sideways and backwards to follow the curve, relying heavily on the linearization of the coupling between body velocities and position.

Figure 5.1 shows the resulting trajectory and tracking errors.

#### Observations

- *Tracking accuracy*: the actual trajectory (solid blue line) closely follows the reference path (dashed black line), almost superimposing on it. Ingenuity manages to transition from the vertical takeoff phase to the periodic figure-8 motion without any noticeable deviation or overshoot.
- *Phases and altitude*: the maneuver begins with a rapid ascent to the target altitude of 5 m: as we can see from the altitude and thrust plots, this aggressive takeoff demands a thrust force significantly higher than the hovering value ( $mg \approx 6.6$  N). The altitude settles at

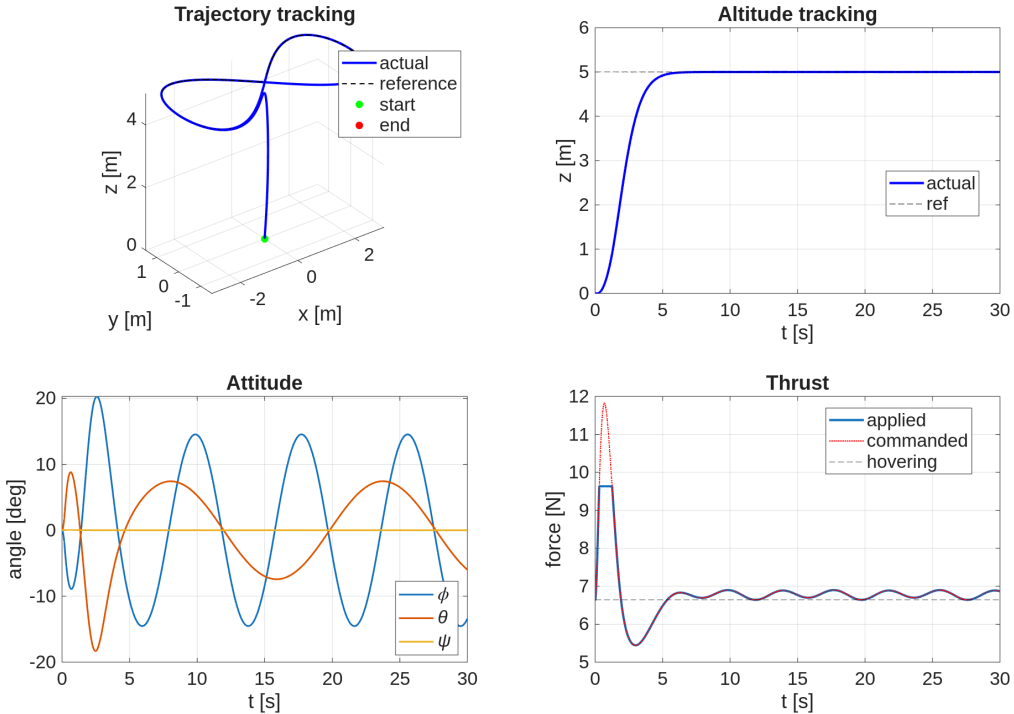


Figure 5.1: Nominal performance on the figure-8 trajectory with constant yaw ( $\psi = 0$ ).

$t \approx 5$  s and remains constant throughout the periodic motion, demonstrating that the DFL controller correctly compensates for the loss of vertical lift when the vehicle tilts to perform lateral maneuvers.

- *Control effort:* from the thrust plot we observe that the commanded thrust (red dotted line) exceeds the physical limit of the actuators during the initial ascent ( $t < 2$  s). The blue line shows the applied thrust being capped at  $F_{\max} \approx 9.6$  N, for a saturation of 13.40%.
- *Attitude:* the roll  $\phi$  and pitch  $\theta$  angles show a clean periodic sinusoidal behavior required to trace the curves, while the yaw  $\psi$  remains constant at zero as expected.

### 5.1.2 Helix trajectory (spinning yaw)

This test is significantly more challenging because Ingenuity ascends while performing a circular motion and simultaneously rotating around its vertical axis ( $\dot{\psi} = 0.5$  rad/s), requiring the controller to constantly adjust the roll and pitch actuation to maintain the correct thrust direction while the body frame is rotating.

Figure 5.2 illustrates the performance.

#### Observations

- *Tracking accuracy:* despite the continuous rotation of the body frame (visible in the attitude plot where  $\psi$  increases linearly), the tracking is excellent. This confirms that the dynamic feedback linearization effectively compensates for the changing orientation of the thrusters relative to the inertial path.

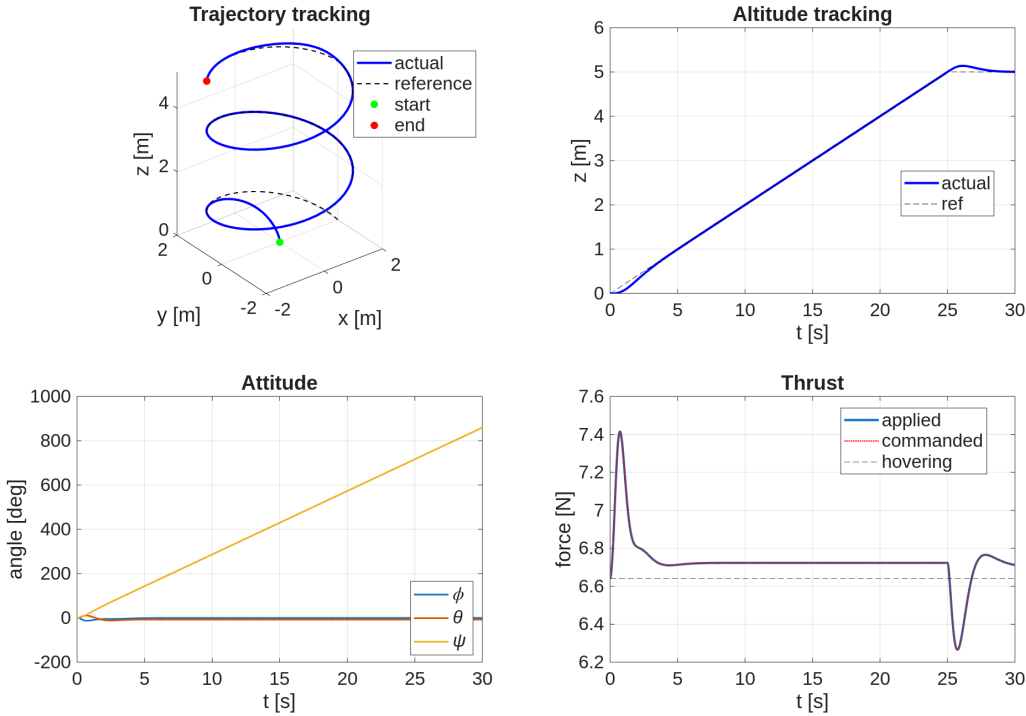


Figure 5.2: Nominal performance on the helix trajectory with spinning yaw.

- *Altitude and thrust:* the altitude tracking follows a linear ramp ( $v_z = 0.2 \text{ m/s}$ ) until  $t = 25 \text{ s}$ . From the thrust plot, we observe an initial pulse to accelerate upwards, a steady-state value slightly above hovering to maintain vertical velocity against drag, and a sharp dip at  $t = 25 \text{ s}$  to arrest the vertical motion and settle at  $z = 5 \text{ m}$ .
- *Actuation:* unlike the previous aggressive takeoff, this smooth ascent keeps the commanded thrust within the physical limits, resulting in no saturation.
- *Attitude:* the controller keeps  $\phi$  and  $\theta$  at small and bounded values necessary to generate the centripetal acceleration for the helix, decoupled from the yaw rotation.

## 5.2 Robustness analysis

Real-world operations on Mars are subject to atmospheric disturbances. To test the robustness of the outer linear tracking loop, we introduce unmodeled wind gusts during the flight.

### 5.2.1 Vertical wind on figure-8

We apply a vertical wind gust (along the inertial  $z$ -axis) while the helicopter tracks the planar figure-8. This specifically stresses the thrust dynamic compensator, as the controller must adapt the total thrust to maintain altitude against an unmodeled lift/downforce.

#### Setup

- **Wind direction:**  $z$ -axis.

- **Intensity:** 2 N ( $\approx 30\%$  of the vehicle's weight).
- **Duration:**  $t \in [10, 15]$  s.

Figure 5.3 shows the system response.

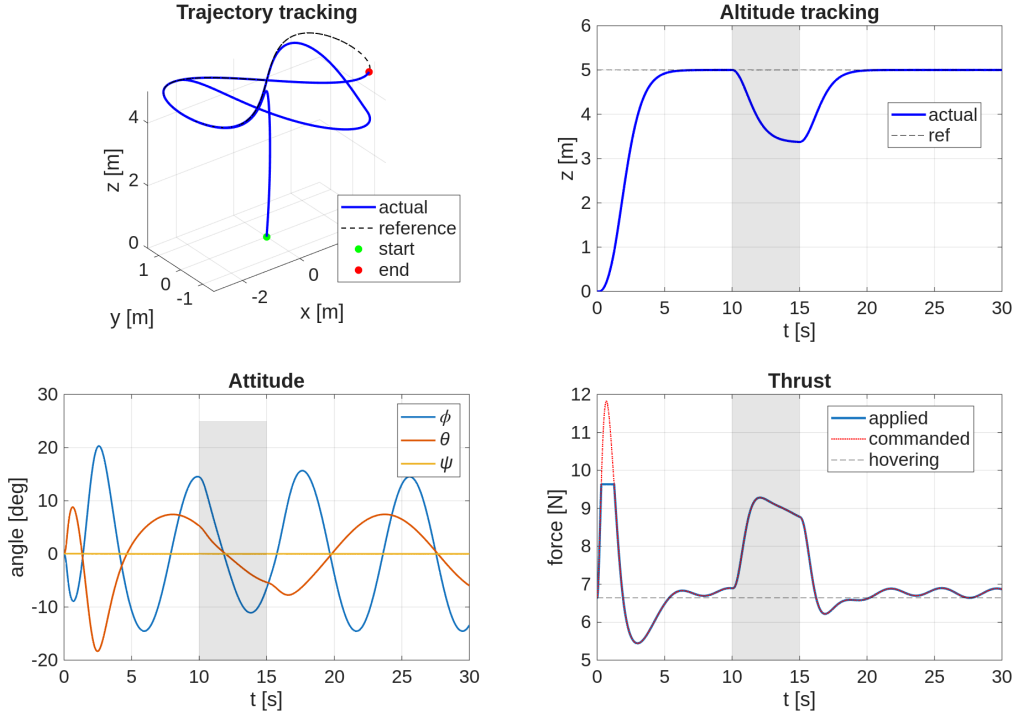


Figure 5.3: Robustness test: figure-8 trajectory with vertical wind gust.

## Observations

- *Altitude deviation:* the unmodeled 2 N downward force causes a sudden altitude drop starting at  $t = 10$  s (indicated by the gray shaded area). The vehicle is pushed down from its setpoint of 5 m to a minimum altitude of approximately 3.4 m before the controller generates enough thrust to arrest the descent.
- *Thrust adaptation:* as the position error increases, the commanded thrust spikes up to around 9.2 N (close to saturation) to counteract the wind and regain altitude.
- *Recovery:* immediately after the wind stops ( $t > 15$  s), the accumulated high thrust causes the drone to accelerate upwards. The controller quickly reduces the power to dampen the motion, resulting in a smooth convergence back to the 5 m setpoint with no overshoot.

### 5.2.2 3D wind on helix

We subject the helicopter to a general wind disturbance acting on all three axes ( $x$ ,  $y$ ,  $z$ ) while tracking the helix trajectory. This tests the ability of the linear outer loops to generate appropriate virtual inputs  $v$  to counteract the drift.

## Setup

- **Wind direction:**  $xyz$ .
- **Intensity:** 2 N.
- **Duration:**  $t \in [8, 11]$  s.

Figure 5.4 illustrates the results.

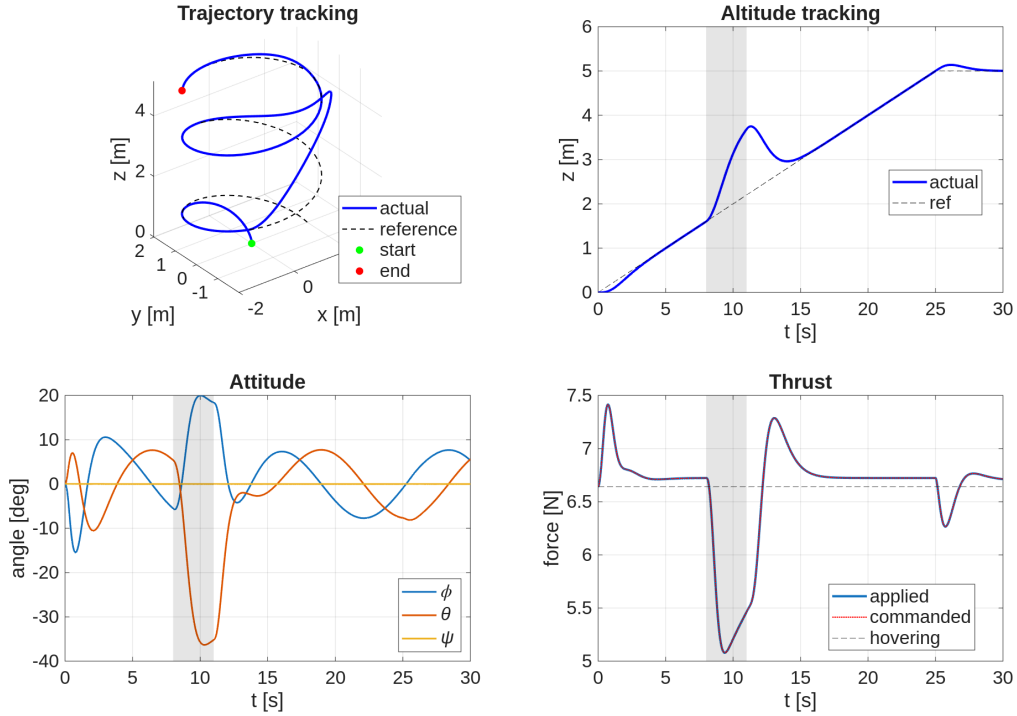


Figure 5.4: Robustness test: helix trajectory with 3D wind gust.

## Observations

- *Transient response:* the altitude plot shows a brief dip during the wind gust, lifting the helicopter off the desired path for a peak error of approximately 2 m.
- *Controller reaction:* the controller reacts by drastically reducing the thrust from  $\approx 6.7$  N down to  $\approx 5.1$  N (below hovering), attempting to use gravity to counter the lift caused by the wind; moreover, the attitude plot shows sharp spikes in  $\phi$  and  $\theta$ , indicating the controller is also tilting the vehicle to generate lateral forces to oppose the horizontal components of the wind.
- *Recovery:* when the wind stops at  $t = 11$  s, the helicopter is left with low thrust and no supporting wind, causing it to rapidly descend. The controller immediately responds with a thrust spike back to  $\approx 7.3$  N to converge back to the reference trajectory, achieving stable flight again by  $t \approx 16$  s.

## 5.3 Complex maneuvering

Finally, we simulate a patrol mission using the box trajectory. Unlike the previous continuous curves, this trajectory involves straight lines connected by sharp 90-degree turns, requiring the vehicle to accelerate, decelerate, and stop accurately.

### 5.3.1 Ideal patrolling (no wind)

We first perform the maneuver in ideal conditions to evaluate the transient response of the controller at the corners.

Figure 5.5 shows the results.

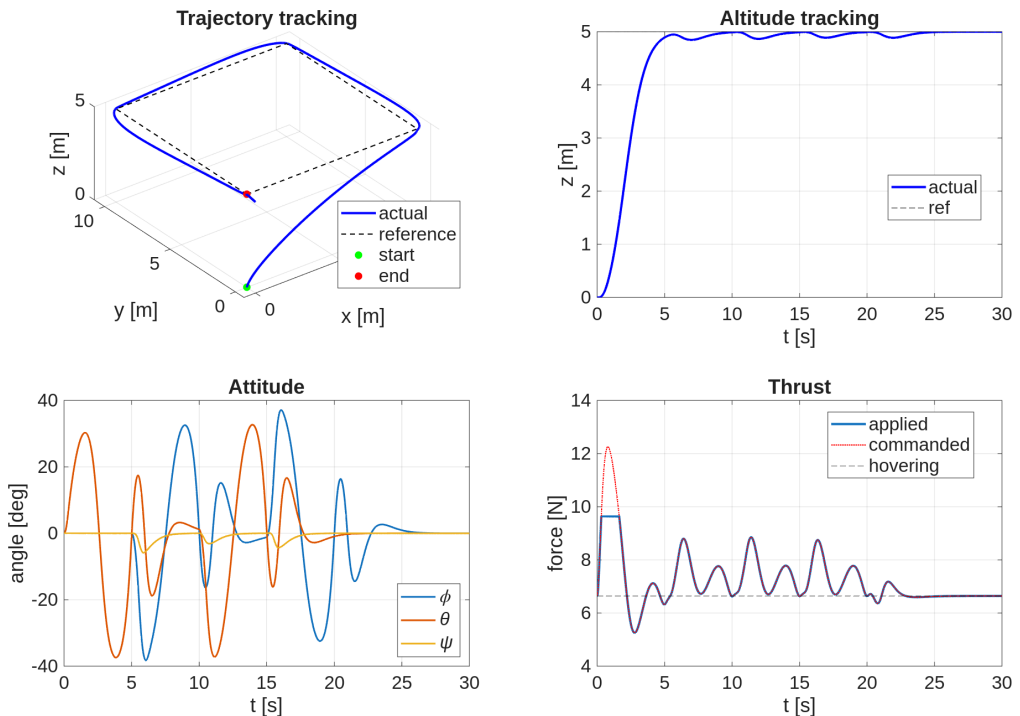


Figure 5.5: Complex maneuvering: box trajectory in ideal conditions.

### Observations

- *Corner performance:* the trajectory tracking plot shows overshoot at the corners of the square path: despite the smoothness of the quintic reference, the inertia of the vehicle prevents an instantaneous turn.
- *Aggressive actuation:* from the thrust and attitude plots we can observe the aggressive nature of the maneuver. The roll and pitch angles spike to nearly  $\pm 40^\circ$  to generate necessary braking and turning forces; similarly, the thrust oscillates significantly between hovering and approximately 9 N.
- *Saturation:* the initial takeoff phase caused the commanded thrust to saturate (5.31% of the flight time). We can also note that the peaks of the oscillations are very close to the physical limit.

### 5.3.2 Patrolling with environmental noise

To simulate a realistic scenario, we repeat the patrol mission with a constant, random wind acting in all directions throughout the entire flight. This represents background atmospheric turbulence rather than a specific strong gust.

Figure 5.6 presents the performance.

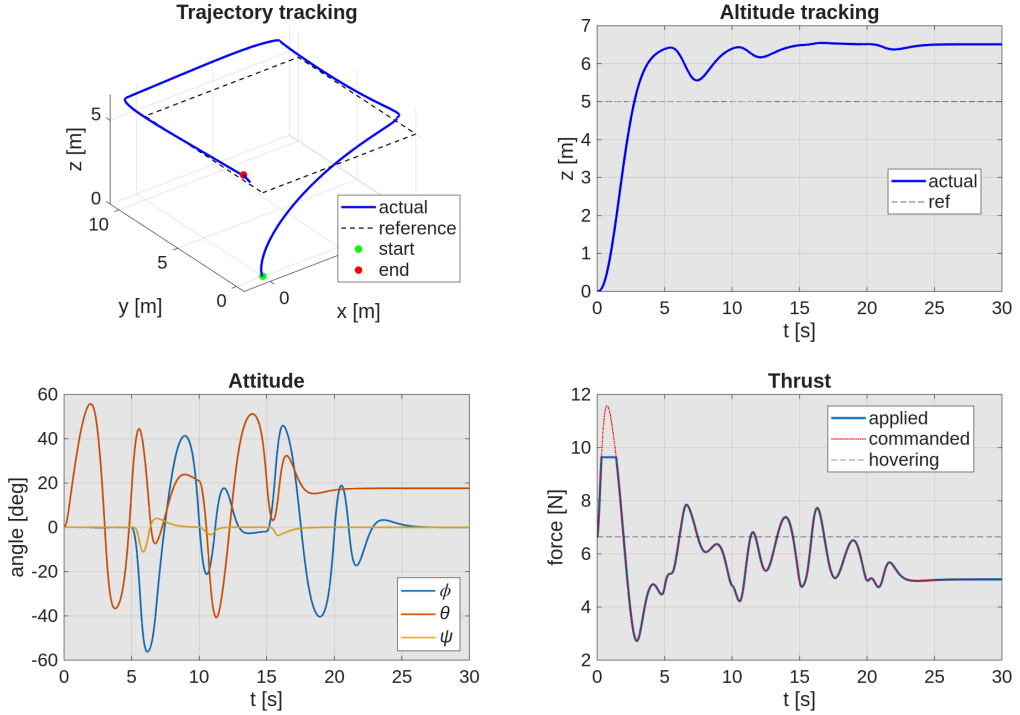


Figure 5.6: Complex maneuvering: box trajectory with continuous environmental disturbance.

### Observations

- *Steady-state drift:* the controller maintains stability and traces the square shape of the patrol; however, there is a noticeable persistent offset from the reference path due to the constant wind: the helicopter hovers at  $z \approx 6.5$  m instead of the desired 5 m, and the 3D plot shows a lateral shift. The maximum tracking error recorded was 5 m.
- *Analysis of the disturbance:* the thrust settles at an unstable value around 6 N, that is lower than hovering because the wind helps to lift the vehicle, and the controller reduces the power to compensate. We can also see how  $\theta$  stabilizes at a non-zero angle ( $\approx 18^\circ$ ) at the end of the flight, indicating Ingenuity is constantly tilted to fight the lateral wind.
- *Saturation:* interestingly, the actuator saturation dropped to 3.64%, lower than the 5.31% of the ideal case. This is consistent with the lower thrust requirement due to the wind “assistance”.

# Chapter 6

## Conclusion

In this project, we analyzed the dynamics of the Ingenuity Mars helicopter and designed a nonlinear control system based on *dynamic feedback linearization* (DFL) to achieve precise trajectory tracking.

### 6.1 Summary

We started by deriving the mathematical model of the co-axial helicopter using Newton-Euler equations. We identified that the system is underactuated and strongly coupled, making standard linear control techniques insufficient. By analyzing the system's input-output dynamics, we determined that the position outputs require four differentiations to reveal the thrust input. Consequently, we designed a dynamic compensator to augment the system state, allowing us to fully linearize the dynamics and decouple the translational and rotational motions.

The proposed controller was validated through simulations in MATLAB under various flight conditions. The results lead to the following conclusions:

- *Nominal performance*: in ideal conditions with perfect model knowledge, the DFL controller achieves excellent tracking accuracy. This was demonstrated in the figure-8 and helix trajectories, where the helicopter followed the reference path with negligible error, even while spinning around its vertical axis.
- *Robustness*: the controlled showed good stability when subjected to temporary wind gusts. Although unmodeled forces caused transient deviations, the outer linear loop successfully stabilized the vehicle back to the reference trajectory once the disturbance ended.
- *Physical limitations*: while DFL assumes unlimited control authority, real actuators have saturation limits which must be taken into account in practical implementations.
- *Steady-state error*: the simulation with continuous environmental noise showed a limitation: while Ingenuity remained stable, the lack of integral action resulted in a constant steady-state offset.

### 6.2 Future work

Based on the findings and limitations observed during this project, several improvements can be explored in future work:

1. *Integral action*: to eliminate the steady-state error observed in the presence of constant wind, the outer-loop PD controller should be upgraded to a PID controller. The integral term would accumulate the error over time and generate the necessary virtual input to cancel out persistent disturbances.
2. *Constraint handling*: DFL does not explicitly handle actuator limits. To prevent saturation during aggressive maneuvers, the reference trajectories could be optimized to respect the physical constraints of the vehicle.
3. *Parameter uncertainty*: DFL relies on exact cancellation of nonlinear terms, which requires precise knowledge of the model parameters (mass, inertia, drag). In a real-world scenario, these parameters are not known perfectly, and an adaptive control law or a robust sliding mode controller (such as passivity-based control) could be implemented to handle parameter uncertainties.
4. *State estimation*: in our simulations we assumed that the full state was perfectly known. In reality, these measurements come from noisy sensors (IMU, cameras) and must be filtered, for example using an *Extended Kalman Filter* (EKF).

# Bibliography

- [1] H. F. Grip, B. Balaram, T. Canham, *et al.*, “Flight control system for nasa’s mars helicopter,” in *AIAA Scitech 2019 Forum*, 2019. DOI: [10.2514/6.2019-1289](https://doi.org/10.2514/6.2019-1289).
- [2] B. Balaram, T. Canham, C. Clark, *et al.*, “Mars helicopter technology demonstrator,” in *2018 AIAA Atmospheric Flight Mechanics Conference*, 2018. DOI: [10.2514/6.2018-0023](https://doi.org/10.2514/6.2018-0023).
- [3] M. Vendittelli, *Quadrotor control via dynamic feedback linearization*, Course Slides, Elective in Robotics, Sapienza University of Rome, 2024.
- [4] M. Vendittelli, *Ingenuity dynamic model (co-axial rotor helicopter)*, Course Slides, Elective in Robotics, Sapienza University of Rome, 2024.